symmetry

MDPI

Article

Cattaneo–Christov Heat Flux Model for Three-Dimensional Rotating Flow of SWCNT and MWCNT Nanofluid with Darcy–Forchheimer Porous Medium Induced by a Linearly Stretchable Surface

Zahir Shah [1], Asifa Tassaddiq [2], Saeed Islam [1], A.M. Alklaibi [3] and Ilyas Khan [4,*]

1 Department of Mathematics, Abdul Wali Khan University, Mardan 23200, Pakistan; zahir1987@yahoo.com (Z.S.); saeedislam@awkum.edu.pk (S.I.)
2 College of Computer and Information Sciences, Majmaah University, Al-Majmaah 11952, Saudi Arabia; a.tassaddiq@mu.edu.sa
3 Department of Mechanical and Industrial Engineering, College of Engineering, Majmaah University, P.O. Box 66 Majmaah 11952, Saudi Arabia; a.alklaibi@mu.edu.sa
4 Faculty of Mathematics and Statistics, Ton Duc Thang University, Ho Chi Minh City 72915, Vietnam
* Correspondence: ilyaskhan@tdt.edu.vn

Received: 2 January 2019; Accepted: 14 February 2019; Published: 6 March 2019

Abstract: In this paper we investigated the 3-D Magnetohydrodynamic (MHD) rotational nanofluid flow through a stretching surface. Carbon nanotubes (SWCNTs and MWCNTs) were used as nano-sized constituents, and water was used as a base fluid. The Cattaneo–Christov heat flux model was used for heat transport phenomenon. This arrangement had remarkable visual and electronic properties, such as strong elasticity, high updraft stability, and natural durability. The heat interchanging phenomenon was affected by updraft emission. The effects of nanoparticles such as Brownian motion and thermophoresis were also included in the study. By considering the conservation of mass, motion quantity, heat transfer, and nanoparticles concentration the whole phenomenon was modeled. The modeled equations were highly non-linear and were solved using homotopy analysis method (HAM). The effects of different parameters are described in tables and their impact on different state variables are displayed in graphs. Physical quantities like Sherwood number, Nusselt number, and skin friction are presented through tables with the variations of different physical parameters.

Keywords: SWCNTs; MWCNTs; stretched surface; rotating system; nanofluid; MHD; thermal radiation; HAM

1. Introduction

Heat transfer phenomenon is important in manufacturing and life science applications, for example in freezing electronics, atomic power plant refrigeration, tissue heat transfer, energy production, etc. Fluids that flow on a stretched surface are more significant among researchers in fields such as manufacturing and commercial processes, for instance in making and withdrawing polymers and gum pieces, crystal and fiber production, food manufacturing, condensed fluid layers, etc. Considering these applications, heat transfer is an essential subject for further investigation in order to develop solutions to stretched surface fluid film problems. The flow of a liquefied sheet was initially considered to obtain a viscid stream and was further extended to stretched surface for non-Newtonian liquids. Choi [1] examined the enhancement of thermal conductivity in nanoparticles deferrals. For the enhancement of thermal conductivity and heat transfer, Hsiao [2,3] performed a

successful survey using the Carreau-Nanofluid and Maxwell models, and obtained some interesting results. Ramasubramaniam et al. [4] treated a homogeneous carbon nanotube composite for electrical purposes. Xue [5] work as presenting a CNT model for grounded compounds. Nasir et al. [6] deliberate the nanofluid tinny liquid flow of SWCNTs using an optimal approach. Ellahi et al. [7] presented the usual transmitting nanofluids based on CNTs. Shah et al. [8,9] investigated nanofluid flow in a rotating frame with microstructural and inertial properties with Hall effects in parallel plates. Hayat and others [10] examined Darcy–Forchheimer flow carbon nanotube flow due to a revolving disk. Recently, scholars have been working on finding a rotational flow close to the flexible or non-expandable geometries due its wide array of uses in rotating-generator systems, food handling, spinning devices, disc cleaners, gas transformer designs, etc. Wang [11] presented a perturbation solution for rotating liquid flow through an elastic sheet. The magnetic flux features of rotating flow above a flexible surface was premeditated by Takhar et al. [12]. Shah et al. [13–15] studied nanofluid and heat transfer with radiative and electrical properties using an optimal approach. Rosali et al. [16] presented a numerical survey for flow with rotation over porous surface with exponential contraction. Hayat et al. [17] used the non-Fourier heat fluctuation hypothesis to get a three-dimensional turning stream of the Jeffrey substances. Mustafa. [18] discussed non-linear aspects of rotating nano-fluid flow through the flexible plane. Sheikholeslami et al. [19] inspected the consistent magnetic and radiated effect on water-based nanofluid in a permeable enclosure. Hsiao [20,21] researched the microploar nanofluid stream with MHD on a stretching surface. Khan et al. [22,23] examined nanofluid of micrpoler fluid with the Darcy–Forchheimer and irregular heat generation/absorption between two plates.

The classical Fourier law of conduction [24] is one best model for explanation of the temperature transmission process under numerous relevant conditions. Cattaneo [25] successfully extended the Fourier model in combining significant properties of the temperature reduction period. Cattaneo's work produced a hyperbolic energy equation for the temperature field which allows heat to be transferred by transmission of heat waves with finite velocity. Heat transfer has many practical applications, from the flow of nanofluids to the simulation of skin burns (see Tibullo and Zampoli [26]). Christov [27] discussed the Cattaneo–Maxwell model for finite heat conduction. Straughan and Ciarletta [28] demonstrated the rareness of the solution of the Cattaneo–Christov equation. Straughan et al. [29] presented the heat transfer analysis for this model with a brief discussion of a solution for the model. Recently, Han et al. [30] deliberated the sliding stream with temperature transmission through the Maxwell fluids for the Christov–Cattaneo model. A numerical comparative survey was also presented for the validation of their described results. The current exploration of nanofluid with entropy analysis can be studied in References [31–36].

This paper is based on the features of the Christov–Cattaneo heat flux in rotating nano liquid. A three-dimensional nanofluid flow is considered over a stretching surface with carbon nanotubes (CNTs). An effective thermal conductivity model was used in the enhancement of heat transfer. The problem was modeled from the schematic diagram with concentration. These modeled equations were transformed into a system of non-linear ordinary differential equations. The modeled equations were coupled and highly non-linear and were tackled by an analytical and numerical approach. Homotopy analysis method (HAM) (a high-precision analytical technique proposed by Liao [37]) was used for the solution of the reduced system. Many researcher [38–46] used HAM due to it to it excellent results. Various parameters are presented via graphs. Different physical parameters (thermal relaxation time, skin friction, etc.) with the variations of other physical constraints are presented via graphs and discussed in detail.

2. Effective Thermal Conductivity Models Available in the Literature

Maxwell's [47] proposed a thermal conductivity model as

$$\frac{k_{nf}}{k_f} = 1 + \frac{3\,(\varsigma - 1)\,\psi}{(\varsigma + 2) - (\varsigma - 1)\,\psi}. \tag{1}$$

where $\varsigma = \frac{k_{nf}}{k_f}$ and ψ is a volumetric fraction. Also, Jeffery [48] proposed the following model:

$$\frac{k_{nf}}{k_f} = 1 + 3\chi\psi + \left(3\chi^2 + \frac{3\chi^2}{4} + \frac{9\chi^3}{16}\left(\frac{\varsigma+2}{2\varsigma+3}\right) + \ldots\ldots\right)\psi^2. \tag{2}$$

where $\chi = \frac{(\varsigma-1)}{(\varsigma+2)}$. After a little modification, Davis [49] presented a model defined as:

$$\frac{k_{nf}}{k_f} = 1 + \frac{3(\varsigma-1)\,\psi}{(\varsigma+2)-(\varsigma-1)\psi}\left\{\psi + \psi(\varsigma)\psi^2 + O(\psi^3)\right\}. \tag{3}$$

This model gives a good approximation of thermal conductivity even for a very small capacity and is independent of the atom's form.

Hamilton and Crosser [50] presented a particle-form-based model defined as:

$$\frac{k_{nf}}{k_f} = \frac{\varsigma + (\hbar-1) - (\varsigma-1)(\hbar-1)\psi}{\varsigma + (\hbar-1) + (1-\varsigma)\psi}. \tag{4}$$

Here $\hbar$ denotes the particle form used. The main limitation of the models discussed above is that they can only be used for rotating or circular components and cannot be used for CNTs, especially for their spatial distribution. To overcome this deficiency, Xue [5] presented a model of very large axel relation and used it for the spatial distribution of CNTs. This model has a mathematical description given as:

$$\frac{k_{nf}}{k_f} = \frac{1-\psi+2\left(\frac{k_{nf}}{k_{nf}-k_f}ln\,\frac{k_{nf}+k_f}{2k_f}\right)\psi}{1-\psi+2\left(\frac{k_f}{k_{nf}-k_f}\,ln\,\frac{k_{nf}+k_f}{2k_f}\right)\psi}. \tag{5}$$

In the present work we implement the Xue [5] model to calculate thermal conductivity.

3. Formulation of the Problem

A three-dimensional rotational flow of CNTs was carried through a linear flexible surface. The temperature distribution was deliberated by the Xue model [5]. The compact fluid describing the Darcy–Forchheimer relationship saturates the permeable area. The stretching surface was adjusted in the Cartesian plane that plates associated in the xy plane. We assumed only the positive values of liquid for z. Surface is extended in the x-direction with a positive rate c. In addition, the liquid is uniformly rotated at a continuous uniform speed ω around the z-axis. Surface temperature is due to convective heating, which is provided by the high temperature of the fluid T_f. The coefficient of this heat transfer is h_f. The relevant equations after applying assumptions are [13–18]:

$$\vec{u}_x + \vec{v}_y + \vec{w}_z = 0 \tag{6}$$

$$u\vec{u}_x + v\vec{u}_y + w\vec{u}_z - 2\omega v = v_{nf}\vec{u}_{zz} - \frac{v_{nf}}{K^*}u - Fu^2 \tag{7}$$

$$u\vec{v}_x + v\vec{v}_y + w\vec{v}_z - 2\omega u = v_{nf}\vec{v}_{zz} - \frac{v_{nf}}{K^*}v - Fv^2 \tag{8}$$

$$\rho c_p\left(uT_x + vT_y + wT_z\right) = -\nabla\cdot\vartheta \tag{9}$$

$$\vartheta + \lambda_2(\vartheta_t + V.\nabla\vartheta - \vartheta.\nabla V + (\nabla.V)\vartheta) = -k\nabla T \tag{10}$$

$$uT_x + vT_y + wT_z = \frac{k}{\rho c_p}T_{zz} - \lambda_2\left[\begin{array}{c} u^2T_{xx} + v^2T_{yy} + w^2T_{zz} + 2uvT_{xy} + 2vwT_{yz} \\ +2uwT_{xz} + \left(u\vec{u}_x + v\vec{u}_y + w\vec{u}_z\right)T_x \\ +\left(u\vec{v}_x + v\vec{v}_y + w\vec{v}_z\right)T_y + \left(u\vec{w}_x + v\vec{w}_y + w\vec{w}_z\right)T_z \end{array}\right] \tag{11}$$

$$u\,C_x + v\,C_y + w\,C_z = D_B\,C_{zz} + \frac{D_T}{T_0}\,T_{zz}. \tag{12}$$

The related boundary conditions are:

$$\begin{gathered} u = u_w(x) = cx, \quad v = 0, \quad w = 0, \quad -k_{nf}T_z = h_f\Big(T_f - T\Big), \\ -k_{nf}C_z = h_f\Big(C_f - C\Big) \quad at \quad z = 0 \\ u \to 0, \quad v \to 0, \quad T \to T_\infty, \quad C \to C_\infty \quad as \quad z \to \infty \end{gathered} \tag{13}$$

K is the permeability, $F = \frac{C_b}{xK^{*1/2}}$ is the irregular inertial coefficient of the permeable medium, C_b represents drag constant and T_∞ represents the ambient fluid temperature. The basic mathematical features of CNTs are [5]:

$$\begin{gathered} \mu_{nf} = \frac{\mu_f}{(1-\phi)^{2.5}},\ v_{nf} = \frac{\mu_{nf}}{\rho_{nf}},\ \alpha_{nf} = \frac{k_{nf}}{(\rho c_p)_{nf}},\ \rho_{nf} = \rho_f(1-\phi) + \rho_{CNT}\phi, \\ (\rho c_p)_{nf} = (\rho c_p)_f(1-\phi) + (\rho c_p)_{CNT}\phi,\ \frac{k_{nf}}{k_f} = \frac{(1-\phi)+2\phi\frac{k_{CNT}}{k_{CNT}-k_f}\ln\frac{k_{CNT}+k_f}{2k_f}}{(1-\phi)+2\phi\frac{k_f}{k_{CNT}-k_f}\ln\frac{k_{CNT}+k_f}{2k_f}} \end{gathered} \tag{14}$$

Transformations are taken as follows:

$$\begin{gathered} u = cxf'(\eta), \quad v = cxg(\eta), \quad w = -(cv_f)^{1/2}f(\eta), \\ \Theta(\eta) = \frac{T-T_\infty}{T_f-T_\infty}, \quad \Phi(\eta) = \frac{C-C_\infty}{C_f-C_\infty}, \quad \eta = \left(\frac{c}{v_f}\right)^{1/2}z. \end{gathered} \tag{15}$$

Now Equation (6) is identically satisfied and Equations (7), (8), (11)–(13) were reduced to

$$\frac{1}{(1-\phi)^{2.5}\left(1-\phi+\frac{\rho_{CNT}}{\rho_f}\phi\right)}\left(f''' - \lambda f'\right) + ff'' + 2Kg - (1+F_r)f'^2 = 0 \tag{16}$$

$$\frac{1}{(1-\phi)^{2.5}\left(1-\phi+\frac{\rho_{CNT}}{\rho_f}\phi\right)}(g'' - \lambda g) + fg' - f'g - 2Kf' - F_r g^2 = 0 \tag{17}$$

$$\frac{k_{nf}}{k_f}\Theta'' + Pr\left[(1-\varphi) + \frac{(\rho c_p)_{nf}}{(\rho c_p)_f}\right]\left[\Theta'\left(\Phi'\right)Nb + \left(\Theta'\right)^2 Nt + f\,\Theta'\right] = 0 \tag{18}$$

$$\Phi'' + Scf\Phi' + \frac{Nt}{Nb}\Theta'' = 0. \tag{19}$$

$$\begin{gathered} f = 0,\ f' = 1,\ g = 0,\ \Theta' = -\frac{k_f}{k_{nf}}\gamma(1-\Theta),\ \Phi' = \frac{k_f}{k_{nf}}\gamma(1-\Phi)\ at\ \eta = 0 \\ f' \to 0,\ g \to 0,\ \Theta \to 0,\ \Phi \to 0, \quad when\ \eta \to \infty \end{gathered} \tag{20}$$

The dimensionless parameters are defined as

$$\begin{gathered} \lambda = \frac{v_f}{cK^*}, \quad F_r = \frac{C_b}{K^{*1/2}}, \quad K = \frac{\omega}{c}, \quad Pr = \frac{v_f}{\alpha_f}, \quad \gamma = \frac{h_f}{k_f}\sqrt{\frac{v_f}{c}}, Sc = \frac{v_f}{D_B}, \\ Pr = \frac{\left(\rho\ c_p\right)_f}{k_f}, Nb = \frac{\tau\ D_B\left(C_f - C_\infty\right)}{v_f}, Nt = \frac{\tau\ D_T\left(T_f - T_\infty\right)}{T_0 v_f}. \end{gathered} \tag{21}$$

where λ represents porosity K rotation parameter, F_r signifies coefficient of is the inertia, Pr, signifies Prandtl number, Nb is the parameter of Brownian motion, Sc signifies Schmidt number, and γ is Biot number and Nt is the thermophoresis parameter which are defined in Equation (21).

4. Results and Discussion

3-D Magnetohydrodynamic (MHD) rotational nanofluid flow through a stretching surface is modeled. The Cattaneo–Christov heat flux model was used for heat transport phenomenon. By considering the conservation of mass, motion quantity, heat transfer, and nanoparticles concentration the whole phenomenon was modeled. The modeled equations were solved using homotopy analysis method (HAM). Figure 1 Show the geometry of the flow pattern.

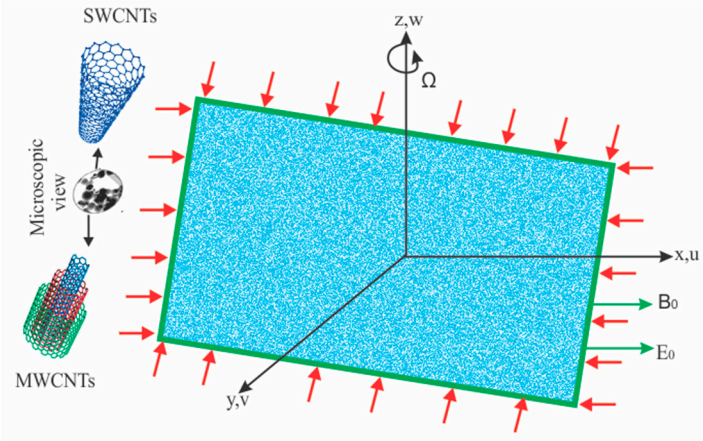

Figure 1. Schematic physical geometry.

Figure 2a–d presents the impact of λ on $f'(\eta)$, $g(\eta)$ & $\Theta(\eta)$ and Biot number γ on $\Theta(\eta)$. Figure 2a displays the deviation of $f'(\eta)$ for different numbers of λ. It was observed that greater porosity parameter λ values indicate a decline in velocity field $f'(\eta)$. Figure 2b reflects the $g(\eta)$ for dissimilar values of the permeability constraint λ. It is detected that for greater permeability constraint λ, the velocity field $g(\eta)$ increased. Figure 2c shows the impact of permeability parameters λ on $\Theta(\eta)$. It is observed that $\Theta(\eta)$ enhanced by increasing the permeability constraint λ for SWCNTs and MWCNTs. Figure 2d illustrates that a greater Biot number γ yields stronger convection, which results in a greater temperature field $\Theta(\eta)$ and hotter sheet wideness.

Figure 3a–d present the impact of K on $f'(\eta)$, $g(\eta)$, $\Theta(\eta)$, and Biot number γ on $\Phi(\eta)$. Figure 3a shows in what way the K affects $f'(\eta)$. A rise in K produced a lesser velocity field $f'(\eta)$ and a smaller momentum sheet wideness of the SWCNTs and MWCNTs. Greater rotational parameter K values resulted in greater rotational rates than tensile rates. Thus, a greater turning effect relates to inferior velocity field $f'(\eta)$ and smaller momentum sheet wideness. Figure 3b describes $g(\eta)$ for K. Larger values of the rotation parameter K, caused a decrease in the velocity field $g(\eta)$. Figure 3c illustrates $\Theta(\eta)$ variations for dissimilar values of K. Greater rotational parameter K decreases the temperature field $\Theta(\eta)$ and supplementary thermal layer width. Figure 3d demonstrates the concentration distribution $\Phi(\eta)$ for varying Biot numbers γ. Higher values of γ indicate enhancement in $\Phi(\eta)$.

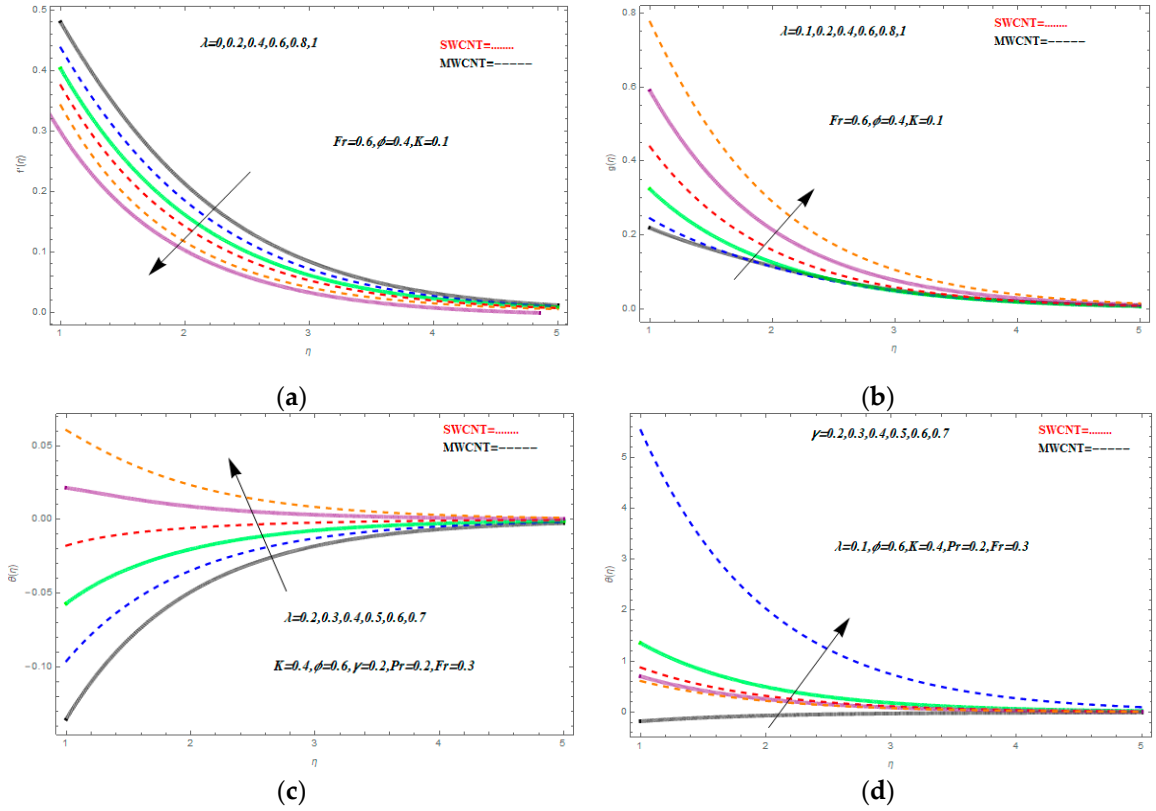

Figure 2. Impression of λ on $f'(\eta)$, $g(\eta)$ & $\Theta(\eta)$, and γ on $\Theta(\eta)$.

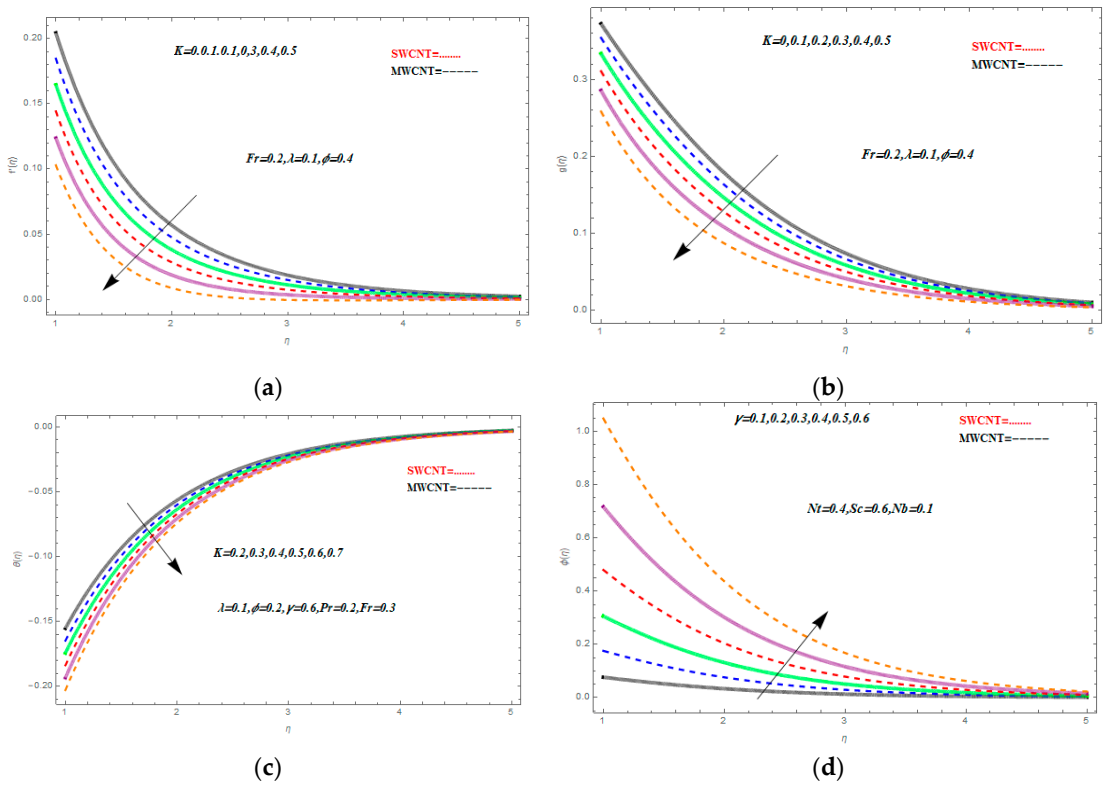

Figure 3. Impression of K on $f'(\eta)$, $g(\eta)$ & $\Theta(\eta)$, and γ on $\Phi(\eta)$.

The influences of inertia coefficient F_r on $f'(\eta)$, $g(\eta)$, $\Theta(\eta)$, and Prandtl number P_r on $\Theta(\eta)$ are shown in Figure 4a–d. Figure 4a shows the inertia coefficient F_r on $f'(\eta)$. It is observed that greater values of inertia coefficients F_r resulted in the decline of $f'(\eta)$. Figure 4b depicts the effect of inertia coefficient F_r over the velocity field $g(\eta)$. For greater inertia coefficients F_r of SWCNTs and MWCNTs, there is an increase in the velocity field $g(\eta)$. The influence of the inertia constant F_r on $\Theta(\eta)$ is shown in Figure 4c. Greater rates of inertia factor F_r resulted in powerful temperature field $\Theta(\eta)$ and additional thermal layer thicknesses for SWCNTs and MWCNTs. Figure 4d shows that greater Prandtl number P_r resulted in the decline of the temperature field $\Theta(\eta)$ of SWCNTs and MWCNTs.

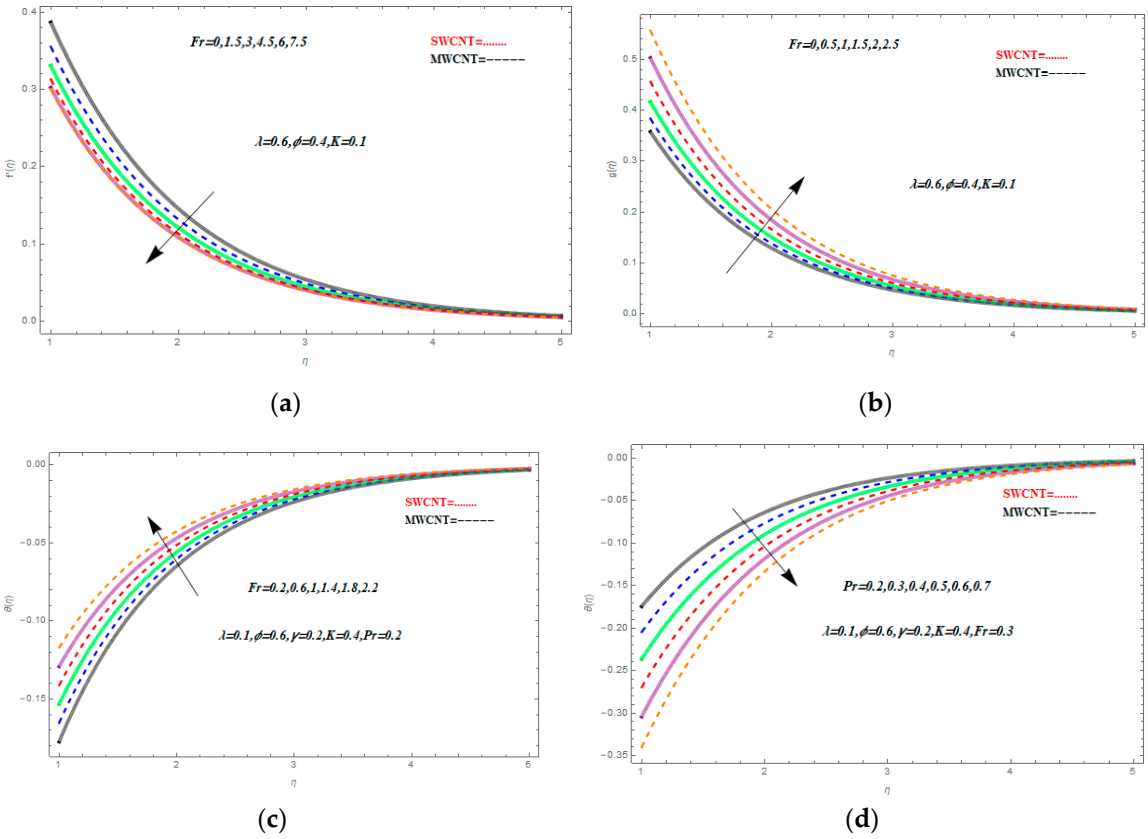

Figure 4. Impression of F_r on $f'(\eta)$, $g(\eta)$, $\Theta(\eta)$, and P_r on $\Theta(\eta)$.

The influences of nanoparticle capacity fraction ϕ on $f'(\eta)$, $g(\eta)$ & $\Theta(\eta)$, Sc on $\Phi(\eta)$ are shown in Figure 5a–d. Figure 5a demonstration the modification in $f'(\eta)$ of the changing nanoparticle capacity fraction ϕ. It was noted that with the rise of the nanoparticle capacity fraction ϕ, an increase $f'(\eta)$ is observed. Results of nanoparticle capacity fraction ϕ on the $g(\eta)$ is shown in Figure 5b. The higher values of the nanoparticle capacity fraction ϕ caused a decreases $g(\eta)$. Figure 5c represents $\Theta(\eta)$ for different nanoparticles volume fraction ϕ. It is observed that greater nanoparticle capacity fraction ϕ resulted in the decline of the temperature field $\Theta(\eta)$. Figure 5d displays the consequence of Sc on $\Phi(\eta)$ of the nanoparticles. It is noticed that an increase in Sc caused a decline in $\Phi(\eta)$.

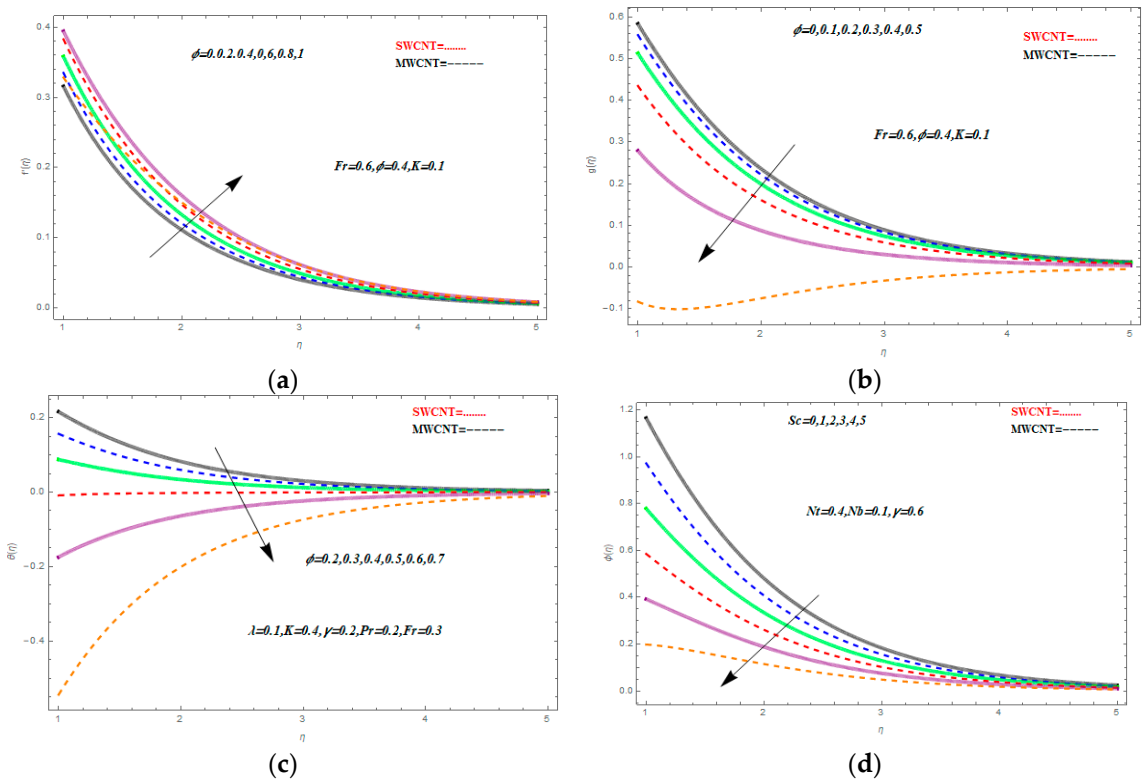

Figure 5. Impression of ϕ on $f'(\eta)$, $g(\eta)$, $\Theta(\eta)$ and Sc on $\Phi(\eta)$.

Figure 6a depicts the concentration distribution $\Phi(\eta)$ for dissimilar values of thermophoretic parameter Nt for SWCNTs and MWCNTs. Higher values of Nt designate the augmentation in $\Phi(\eta)$. Figure 6b depicts the concentration distribution $\Phi(\eta)$ for the varying Brownian motion parameter Nb of SWCNTs and MWCNTs. We noted that greater values of Nb show a reduction in $\Phi(\eta)$ and the connected boundary film thickness.

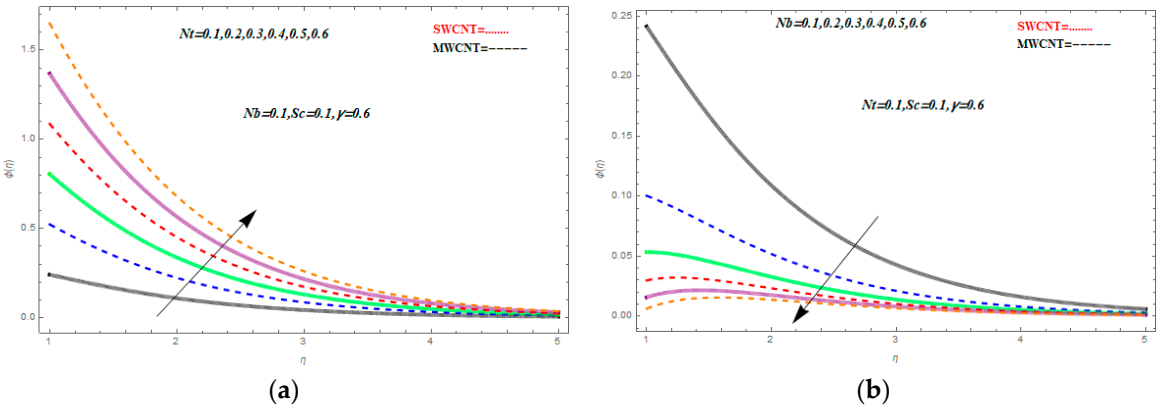

Figure 6. Impression of Nt on $\Theta(\eta)$ and Nb. on $\Phi(\eta)$.

4.1. Table Discussion

Physical values of skin friction for dissimilar values of SWCNTs and MWCNTs in the case of different parameters for C_{fx} and C_{fy} are calculated numerically in Table 1. It was perceived that amassed values of F_r, λ and γ increasing C_{fx} and C_{fy} for SWCNTs nanofluid. Similar results were obtained for MWCNTs. The higher value of K reduces C_{fx} and C_{fy} for SWCNT nanofluid, while for MWCNTs the result was opposite. Physical values for the heat and mass fluxes for dissimilar

parameters at $Pr = 7.0$ are calculated in Table 2. Greater values of F_r and K augmented the heat flux as well as the mass flux for both SWCNTs and MWCNTs. The higher value of Nt and Nb reduced the heat flux as well as the mass flux while increasing γ decreased it for both SWCNTs and MWCNTs.

Table 1. Variation in skin friction.

F_r	K	λ	γ	$-C_{fx}$		$-C_{fy}$	
				SWCNT	**MWCNT**	**SWCNT**	**MWCNT**
0.0	0.1	0.1	0.1	1.08621	1.03466	1.24014	1.14536
0.1	–	–	–	1.15376	1.12687	1.27592	1.19880
0.3	–	–	–	1.19736	1.14350	1.34626	1.24368
0.1	0.0	–	–	1.19574	1.04576	1.19574	1.13667
–	0.3	–		0.98487	0.23571	1.44073	1.17462
–	0.5	–	–	0.85351	0.02547	1.61115	1.32445
–	0.1	0.0	–	0.96939	0.23419	1.10121	1.03462
–	–	0.3	–	1.54123	1.45483	1.23261	1.100344
–	–	0.5	–	1.68412	1.52445	1.69793	1.37352
–	–	0.1	0.1	1.69222	1.57245	1.72350	1.22359
–	–	–	0.3	1.73432	1.62355	1.88193	1.31912
–	–	–	0.5	1.92365	1.81199	1.90843	1.59331

Table 2. Variation in Nusselt number and Sherwood Number at $Pr = 7.0$.

F_r	K	Nt	Nb	γ	$-Nu_x$		$-Sh_x$	
					SWCNT	**MWCNT**	**SWCNT**	**MWCNT**
0.0	0.1	0.1	0.1	0.1	0.116964	0.231567	0.120208	0.243362
0.1	–	–	–	–	0.116964	0.231390	0.120212	0.243021
0.3	–	–	–	–	0.116965	0.233321	0.120212	0.243204
0.1	0.0	–	–	–	0.116965	0.134136	0.120202	0.243204
–	0.3	–	–	–	0.116966	0.134342	0.120196	0.243192
–	0.5	–	–	–	0.116967	0.134351	0.128786	0.243145
–	0.1	0.3	–	–	0.116953	0.261532	0.13737	0.243145
–	–	0.5	–	–	0.116943	0.261531	0.15026	0.950126
–	–	0.8	–	–	0.116926	0.261530	0.118472	0.950139
–	–	0.1	0.5	–	0.118451	0.156382	0.116457	0.936457
–	–	–	1.0	–	0.120623	0.234521	0.114607	0.934607
–	–	–	1.5	–	0.122502	0.267373	0.11678	0.932678
–	–	–	0.1	0.5	0.116945	0.234536	0.116352	0.566352
–	–	–	–	1.0	0.116928	0.198342	0.116209	0.566209
–	–	–	–	1.5	0.116895	0.162455	0.116198	0.526198

5. Conclusions

Three-dimensional MHD rotational flow of nanofluid over a stretching surface with Cattaneo–Christov heat flux was numerically investigated. Nanofluid is formed as a suspension of SWCNTs and MWCNTs. The modeled equations under different physical parameters were analyzed via graphs for SWNTs. The following main points were concluded from this work.

- It was observed that greater porosity parameter λ values reduced $f'(\eta)$ while increasing $g(\eta)$ and also increasing temperature field $\Theta(\eta)$ for SWCNTs and MWCNTs.
- Greater Biot number γ yields stronger convection, which results in a greater temperature field $\Theta(\eta)$ and hotter sheet wideness.
- Greater rotational parameter K values resulted in greater rotational rates than tensile rates. The higher value of K increased the fluid velocity.
- It was observed that greater values of inertia coefficients F_r resulted in the decline of the velocity field.
- The higher value of the nanoparticle capacity fraction ϕ increased the velocity field and decreased temperature.
- Higher values of Nt indicated enhancement in $\Phi(\eta)$.
- Greater values of Nb showed reduction in $\Phi(\eta)$.
- Larger values of Sc demoted nanoparticle concentration $\Phi(\eta)$.
- It was perceived that increasing values of F_r, λ, and γ increased C_{fx} and C_{fy} for SWCNT nanofluid. Similar results were obtained for MWCNTs.
- The higher values of Nt and Nb reduced the heat flux as well as the mass flux, while increasing γ decreased it for both SWCNTs and MWCNTs.

Author Contributions: Z.S. and S.I. modeled the problem and wrote the manuscript. A.T. and I.K. thoroughly checked the mathematical modeling and English corrections. Z.S. and A.M.A. solved the problem using Mathematica software. I.K., S.A. and A.T. contributed to the results and discussions. All authors finalized the manuscript after its internal evaluation.

Funding: This research received no external funding.

Conflicts of Interest: The authors declare no conflict of interest.

References

1. Choi, S.U.S.; Zhang, Z.G.; Yu, W.; Lockwood, F.E.; Grulke, E.A. Anomalous thermal conductivity enhancement in nanotube suspensions. *Appl. Phys. Lett.* **2001**, *79*, 2252–2254. [CrossRef]
2. Hsiao, K. To promote radiation electrical MHD activation energy thermal extrusion manufacturing system efficiency by using Carreau-Nanofluid with parameters control method. *Energy* **2017**, *130*, 486–499. [CrossRef]
3. Hsiao, K. Combined Electrical MHD Heat Transfer Thermal Extrusion System Using Maxwell Fluid with Radiative and Viscous Dissipation Effects. *Appl. Therm. Eng.* **2017**, *112*, 1281–1288. [CrossRef]
4. Shah, Z.; Dawar, A.; Islam, S.; Khan, I.; Ching, D.L.C. Darcy-Forchheimer Flow of Radiative Carbon Nanotubes with Microstructure and Inertial Characteristics in the Rotating Frame. *Case Stud. Therm. Eng.* **2018**, *12*, 823–832. [CrossRef]
5. Xue, Q.Z. Model for thermal conductivity of carbon nanotube-based composites. *Phys. B Condens. Matter* **2005**, *368*, 302–307. [CrossRef]
6. Nasir, N.; Shah, Z.; Islam, S.; Bonyah, E.; Gul, T. Darcy Forchheimer nanofluid thin film flow of SWCNTs and heat transfer analysis over an unsteady stretching sheet. *AIP Adv.* **2019**, *9*, 015223. [CrossRef]
7. Ellahi, R.; Hassan, M.; Zeeshan, A. Study of natural convection MHD nanofluid by means of single and multi-walled carbon nanotubes suspended in a salt-water solution. *IEEE Trans. Nanotechnol.* **2015**, *14*, 726–734. [CrossRef]
8. Shah, Z.; Islam, S.; Ayaz, H.; Khan, S. The electrical MHD and hall current impact on micropolar nanofluid flow between rotating parallel plates. *Results Phys.* **2018**, *9*, 1201–1214. [CrossRef]
9. Shah, Z.; Islam, S. Radiative heat and mass transfer analysis of micropolar nanofluid flow of Casson fluid between two rotating parallel plates with effects of Hall current. *ASME J. Heat Transf.* **2019**, *141*, 022401. [CrossRef]
10. Hayat, T.; Haider, F.; Muhammad, T.; Alsaedi, A. On Darcy-Forchheimer flow of carbon nanotubes due to a rotating disk. *Int. J. Heat Mass Transf.* **2017**, *112*, 248–254. [CrossRef]

11. Wang, C.Y. Stretching a surface in a rotating fluid. *Zeitschrift für angewandte Mathematik und Physik ZAMP* **1988**, *39*, 177–185. [CrossRef]
12. Takhar, H.S.; Chamkha, A.J.; Nath, G. Flow and heat transfer on a stretching surface in a rotating fluid with a magnetic field. *Int. J. Therm. Sci.* **2003**, *42*, 23–31. [CrossRef]
13. Shah, Z.; Bonyah, E.; Islam, S.; Gul, T. Impact of thermal radiation on electrical mhd rotating flow of carbon nanotubes over a stretching sheet. *Aip Adv.* **2019**, *9*, 015115. [CrossRef]
14. Shah, Z.; Dawar, A.; Islam, S.; Khan, I.; Ching, D.L.C.; Khan, Z.A. Cattaneo-Christov model for Electrical MagnetiteMicropoler Casson Ferrofluid over a stretching/shrinking sheet using effective thermal conductivity model. *Case Stud. Therm. Eng.* **2018**. [CrossRef]
15. Shah, Z.; Gul, T.; Khan, A.M.; Ali, I.; Islam, S. Effects of hall current on steady three dimensional non-newtonian nanofluid in a rotating frame with brownian motion and thermophoresis effects. *J. Eng. Technol.* **2017**, *6*, 280–296.
16. Rosali, H.; Ishak, A.; Nazar, R.; Pop, I. Rotating flow over an exponentially shrinking sheet with suction. *J. Mol. Liquids* **2015**, *211*, 965–969. [CrossRef]
17. Hayat, T.; Qayyum, S.; Imtiaz, M.; Alsaedi, A. Three-dimensional rotating flow of Jeffrey fluid for Cattaneo-Christov heat flux model. *AIP Adv.* **2016**, *6*, 025012. [CrossRef]
18. Mustafa, M.; Mushtaq, A.; Hayat, T.; Alsaedi, A. Rotating flow of magnetite-water nanofluid over a stretching surface inspired by non-linear thermal radiation. *PLoS ONE* **2016**, *11*, e0149304. [CrossRef] [PubMed]
19. Sheikholeslami, M.; Shah, Z.; Shafi, A.; Khan, I.; Itili, I. Uniform magnetic force impact on water based nanofluid thermal behavior in a porous enclosure with ellipse shaped obstacle. *Sci. Rep.* **2019**, *9*, 1196. [CrossRef] [PubMed]
20. Hsiao, K. Micropolar Nanofluid Flow with MHD and Viscous Dissipation Effects Towards a Stretching Sheet with Multimedia Feature. *Int. J. Heat Mass Transf.* **2017**, *112*, 983–990. [CrossRef]
21. Hsiao, K. Stagnation Electrical MHD Nanofluid Mixed Convection with Slip Boundary on a Stretching Sheet. *Appl. Therm. Eng.* **2016**, *98*, 850–861. [CrossRef]
22. Khan, A.; Shah, Z.; Islam, S.; Khan, S.; Khan, W.; Khan, Z.A. Darcy–Forchheimer flow of micropolar nanofluid between two plates in the rotating frame with non-uniform heat generation/absorption. *Adv. Mech. Eng.* **2018**, *10*, 1–16. [CrossRef]
23. Khan, A.; Shah, Z.; Islam, S.; Dawar, A.; Bonyah, E.; Ullah, H.; Khan, Z.A. Darcy-Forchheimer flow of MHD CNTs nanofluid radiative thermal behaviour andconvective non uniform heat source/sink in the rotating frame with microstructureand inertial characteristics. *AIP Adv.* **2018**, *8*, 125024. [CrossRef]
24. Fourier, J. Theorie Analytique de la Chaleur, par M. Fourier; Chez Firmin Didot, père et Fils. 1822. Available online: https://gallica.bnf.fr/ark:/12148/bpt6k1045508v.texteImage (accessed on 1 January 2019).
25. Cattaneo, C. Sulla conduzione del calore. *Atti Sem. Mat. Fis. Univ. Modena* **1948**, *3*, 83–101.
26. Tibullo, V.; Zampoli, V. A uniqueness result for the Cattaneo–Christov heat conduction model applied to incompressible fluids. *Mech. Res. Commun.* **2011**, *38*, 77–79. [CrossRef]
27. Christov, C.I. On frame indifferent formulation of the Maxwell–Cattaneo model of finite-speed heat conduction. *Mech. Res. Commun.* **2009**, *36*, 481–486. [CrossRef]
28. Straughan, B. Thermal convection with the Cattaneo–Christov model. *Int. J. Heat Mass Transf.* **2010**, *53*, 95–98. [CrossRef]
29. Ciarletta, M.; Straughan, B. Uniqueness and structural stability for the Cattaneo–Christov equations. *Mech. Res. Commun.* **2010**, *37*, 445–447. [CrossRef]
30. Han, S.; Zheng, L.; Li, C.; Zhang, X. Coupled flow and heat transfer in viscoelastic fluid with Cattaneo–Christov heat flux model. *Appl. Math. Lett.* **2014**, *38*, 87–93. [CrossRef]
31. Feroz, N.; Shah, Z.; Islam, S.; Alzahrani, E.O.; Khan, W. Entropy Generation of Carbon Nanotubes Flow in a Rotating Channel with Hall and Ion-Slip Effect Using Effective Thermal Conductivity Model. *Entropy* **2019**, *21*, 52. [CrossRef]
32. Alharbi, S.O.; Dawar, A.; Shah, Z.; Khan, W.; Idrees, M.; Islam, S.; Khan, I. Entropy Generation in MHD Eyring–Powell Fluid Flow over an Unsteady Oscillatory Porous Stretching Surface under the Impact of Thermal Radiation and Heat Source/Sink. *Appl. Sci.* **2018**, *8*, 2588. [CrossRef]
33. Khan, N.S.; Shah, Z.; Islam, S.; Khan, I.; Alkanhal, T.A.; Tlili, I. Entropy Generation in MHD Mixed Convection Non-Newtonian Second-Grade Nanoliquid Thin Film Flow through a Porous Medium with Chemical Reaction and Stratification. *Entropy* **2019**, *21*, 139. [CrossRef]

34. Ishaq, M.; Ali, G.; Shah, Z.; Islam, S.; Muhammad, S. Entropy Generation on Nanofluid Thin Film Flow of Eyring–Powell Fluid with Thermal Radiation and MHD Effect on an Unsteady Porous Stretching Sheet. *Entropy* **2018**, *20*, 412. [CrossRef]
35. Dawar, A.; Shah, Z.; Khan, W.; Idrees, M.; Islam, S. Unsteady squeezing flow of MHD CNTS nanofluid in rotating channels with Entropy generation and viscous Dissipation. *Adv. Mech. Eng.* **2019**, *10*, 1–18. [CrossRef]
36. Sheikholeslami, M.; Shah, Z.; Tassaddiq, A.; Shafee, A.; Khan, I. Application of Electric Field for Augmentation of Ferrofluid Heat Transfer in an Enclosure including Double Moving Walls. *IEEE Access* **2019**. [CrossRef]
37. Liao, S. Notes on the homotopy analysis method: Some definitions and theorems. *Commun. Nonlinear Sci. Numer. Simul.* **2009**, *14*, 983–997. [CrossRef]
38. Shah, Z.; Bonyah, E.; Islam, S.; Khan, W.; Ishaq, M. Radiative MHD thin film flow of Williamson fluid over an unsteady permeable stretching. *Heliyon* **2018**, *4*, e00825. [CrossRef] [PubMed]
39. Jawad, M.; Shah, Z.; Islam, S.; Islam, S.; Bonyah, E.; Khan, Z.A. Darcy-Forchheimer flow of MHD nanofluid thin film flow with Joule dissipation and Navier's partial slip. *J. Phys. Commun.* **2018**. [CrossRef]
40. Khan, N.; Zuhra, S.; Shah, Z.; Bonyah, E.; Khan, W.; Islam, S. Slip flow of Eyring-Powell nanoliquid film containing graphene nanoparticles. *AIP Adv.* **2018**, *8*, 115302. [CrossRef]
41. Fiza, M.; Islam1, S.; Ullah, H.; Shah, Z.; Chohan, F. An Asymptotic Method with Applications to Nonlinear Coupled Partial Differential Equations. *Punjab Univ. J. Math.* **2018**, *50*, 139–151.
42. Ali, A.; Sulaiman, M.; Islam, S.; Shah, Z.; Bonyah, E. Three-dimensional magnetohydrodynamic (MHD) flow of Maxwell nanofl uid containing gyrotactic micro-organisms with heat source/sink. *AIP Adv.* **2018**, *8*, 085303. [CrossRef]
43. Dawar, A.; Shah, Z.; Idrees, M.; Khan, W.; Islam, S.; Gul, T. Impact of Thermal Radiation and Heat Source/Sink on Eyring–Powell Fluid Flow over an Unsteady Oscillatory Porous Stretching Surface. *Math. Comput. Appl.* **2018**, *23*, 20. [CrossRef]
44. Hammed, K.; Haneef, M.; Shah, Z.; Islam, I.; Khan, W.; Asif, S.M. The Combined Magneto hydrodynamic and electric field effect on an unsteady Maxwell nanofluid Flow over a Stretching Surface under the Influence of Variable Heat and Thermal Radiation. *Appl. Sci.* **2018**, *8*, 160. [CrossRef]
45. Khan, A.S.; Nie, Y.; Shah, Z.; Dawar, A.; Khan, W.; Islam, S. Three-Dimensional Nanofluid Flow with Heat and Mass Transfer Analysis over a Linear Stretching Surface with Convective Boundary Conditions. *Appl. Sci.* **2018**, *8*, 2244. [CrossRef]
46. Maxwell, J.C. *Electricity and Magnetism*, 3rd ed.; Clarendon: Oxford, UK, 1904.
47. Jawad, M.; Shah, Z.; Islam, S.; Majdoubi, J.; Tlili, I.; Khan, W.; Khan, I. Impact of Nonlinear Thermal Radiation and the Viscous Dissipation Effect on the Unsteady Three-Dimensional Rotating Flow of Single-Wall Carbon Nanotubes with Aqueous Suspensions. *Symmetry* **2019**, *11*, 207. [CrossRef]
48. Jeffrey, D.J. Conduction through a random suspension of spheres. *Proc. R. Soc. Lond. A* **1973**, *335*, 355–367. [CrossRef]
49. Davis, R.H. The effective thermal conductivity of a composite material with spherical inclusions. *Int. J. Thermophys.* **1986**, *7*, 609–620. [CrossRef]
50. Hamilton, R.L.; Crosser, O.K. Thermal conductivity of heterogeneous two-component systems. *Ind. Eng. Chem. Fundam.* **1962**, *1*, 187–191. [CrossRef]